Accurate Reactive Power Sharing in an Islanded Microgrid Using Adaptive Virtual Impedances

Hisham Mahmood, *Student Member, IEEE*, Dennis Michaelson, *Member, IEEE*, and Jin Jiang, *Senior Member, IEEE*

***Abstract*—In this paper, a reactive power sharing strategy that employs communication and the virtual impedance concept is proposed to enhance the accuracy of reactive power sharing in an islanded microgrid. Communication is utilized to facilitate the tuning of adaptive virtual impedances in order to compensate for the mismatch in voltage drops across feeders. Once the virtual impedances are tuned for a given load operating point, the strategy will result in accurate reactive power sharing even if communication is disrupted. If the load changes while communication is unavailable, the sharing accuracy is reduced, but the proposed strategy will still outperform the conventional droop control method. In addition, the reactive power sharing accuracy based on the proposed strategy is immune to the time delay in the communication channel. The sensitivity of the tuned controller parameters to changes in the system operating point is also explored. The control strategy is straightforward to implement and does not require knowledge of the feeder impedances. The feasibility and effectiveness of the proposed strategy are validated using simulation and experimental results from a 2-kVA microgrid.**

***Index Terms*—Droop control, microgrid control, reactive power control, virtual impedance.**

I. Introduction

Distributed generation (DG) has recently received a great deal of attention as a potential solution to meet the increased demand for electricity, to reduce stress on the existing transmission system, and to incorporate more renewable and alternative energy sources. Subsequently, the microgrid concept has emerged as a promising approach to coordinate different types of distributed energy resources effectively by using local power management systems. A microgrid also allows the DG units to work in an islanded configuration, and therefore improves the availability and quality of power supplied to customers [1]. However, islanded microgrids exhibit challenging control problems, such as the difficulty of maintaining generation/load power balance and reactive power sharing.

When a microgrid is operating in the islanded mode each DG unit should be able to supply its share of the total load in proportion to its rating. To achieve this, frequency and voltage droop control techniques that mimic the behavior of synchronous machines in conventional power systems are widely adopted in the literature [2]–[8]. The reason for the popularity of the droop control technique is that it provides a decentralized control capability that does not depend on external communication links in the control strategy—this enables "plug-and-play" interfacing [3] and enhances the reliability of the system. Communication can, however, be used in addition to the droop control method to enhance the system performance without reducing reliability [9]–[15].

Although the frequency droop technique can achieve accurate real power sharing, the voltage droop technique typically results in poor reactive power sharing due to the mismatch in the impedances of the DG unit feeders and, also, due to the different ratings of the DG units [16]. Consequently, the problem of reactive power sharing in islanded microgrids has received considerable attention in the literature and many control techniques have been developed to address this issue [17]–[30].

A comprehensive treatment of the virtual impedance concept to mitigate errors in reactive power sharing is presented in [17]–[19]. The focus has been on the mismatch in the output impedances of the closed-loop controlled inverters that are used to interface the DG units. With proper design of the voltage controller, the closed-loop output impedances must be negligible at steady state around the nominal operating frequency. Therefore, the virtual impedance is dominant, which results in accurate reactive power sharing. However, the analysis in [17]–[19] did not consider the mismatch in the physical impedance of the feeders, including transformers, cables, and the interface inductors associated with each unit.

A unique approach is proposed in [20] to achieve accurate reactive power sharing. The proposed strategy requires injection of a small ac voltage signal in the system. Overlaying such an ac voltage signal may reduce the quality of the output voltage and line current [21], [24]. Also, extracting and processing this signal may result in a complicated implementation, particularly in a noisy environment.

A control strategy employing an inductive virtual impedance is developed in [21] to ensure accurate reactive power sharing. The proposed analysis and design is based on the assumption that the feeder impedance is small and dominated by the virtual impedance, which is a known parameter. Moreover, the feeder physical impedance is estimated to improve the accuracy, and to include the effect of the impedance resistive component. The estimation technique requires the system to operate in grid connected mode first, before islanding. The technique is validated for a system with different virtual impedances, but with identical feeder physical impedances. On the other hand, the analysis and the control strategy introduced in [22] requires that the feeder

Manuscript received November 3, 2013; revised February 17, 2014; accepted March 17, 2014. Date of publication April 1, 2014; date of current version October 15, 2014. Recommended for publication by Associate Editor Y. Sozer.

The authors are with the Department of Electrical and Computer Engineering, University of Western Ontario, London, ON N6A 5B9, Canada (e-mail: hmahmoo2@uwo.ca; dgm@uwo.ca; jjiang@eng.uwo.ca).

Color versions of one or more of the figures in this paper are available online at http://ieeexplore.ieee.org.

Digital Object Identifier 10.1109/TPEL.2014.2314721

impedances are resistive. The analysis and the control strategy results in accurate power sharing if this condition is satisfied. In practice, however, the feeders may have both nonnegligible inductive and resistive components [17].

Control strategies are proposed in [23] and [29] to achieve accurate power sharing among the inverters in an islanded microgrid. When the inverters are in close proximity an instantaneous control interconnection becomes feasible and can be used as an essential component to achieve accurate sharing. In practice, the DG units might be located in different geographic locations making this approach ineffective.

An interesting control strategy is proposed in [24]. The control strategy is composed of two stages: An initial conventional droop-based control stage and a synchronized compensation stage. During the synchronized compensation stage, the frequency droop is used to control the reactive power sharing. Since this action will also disturb the real power sharing, an integral control term is added to the voltage droop to maintain real power sharing accuracy. However, load changes during the compensation period or between compensation periods may result in poor power sharing.

Communication is used in [25] to facilitate the estimation of the feeder impedances which are then used to set the virtual impedances to ensure accurate reactive power sharing. The feeder impedance is estimated at the local DG controller by utilizing the point of common coupling (PCC) voltage harmonic data transferred via a communication link. This is based on the assumption that the phase angle difference between the voltages at the PCC and at the inverter output is negligible. This assumption may not hold for long feeders or for higher power levels. The same technique is used in [26] under the same assumption.

Communication links are also used in [27] to enhance the performance of conventional droop control. The proposed technique can reduce the sharing error but cannot eliminate it completely. For example, it reduces the maximum sharing error from 5.02 % to 3.05 %. Also, the performance of the technique is sensitive to delays in communication; e.g., a delay of 16 ms degrades the sharing accuracy significantly. A new droop control is proposed in [28] to reduce the power sharing error. As in [27], the sharing error can be reduced but not completely eliminated and the improvement in performance is not significant if local loads are connected at the output of each unit.

A distributed secondary control technique is proposed in [30] to restore the frequency and the voltage, and also to ensure accurate reactive power sharing. In this technique, the controller is implemented in each DG unit instead of implementing it in the microgrid central energy management unit. Communication data drop-outs/packet losses are briefly discussed in the paper, however the scenario of a complete communication failure is not investigated.

In this paper, a control strategy that employs communication is proposed to enhance reactive power sharing accuracy. Communication is utilized to tune the adaptive virtual impedances in order to compensate for the mismatch in voltage drops across feeders. Once the virtual impedances are tuned for a given load operating point, the strategy will result in accurate reactive power sharing even if the communication is disrupted. If the load changes while communication is unavailable, the proposed strategy will still outperform conventional droop control. The control strategy is straightforward to implement and does not require knowledge of the feeder impedances. Also, the reactive power sharing accuracy based on the proposed strategy is immune to time delays in the communication channel.

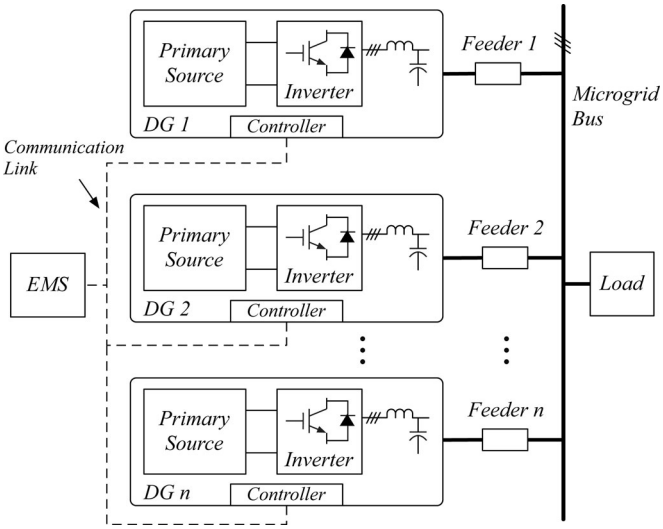

Fig. 1. Islanded microgrid with communication links to an energy management system (EMS).

In Section II of this paper, an overview of the system structure is presented along with an explanation of how reactive power is conventionally shared. The proposed controller is introduced in Section III along with a discussion of the controller sensitivity to the operating point and discussion of the communication mechanism. Simulation and experimental results based on the proposed strategy are presented in Sections IV and V, respectively, followed by concluding remarks in Section VI.

II. Islanded Microgrid Structure and Control

A. Islanded Microgrid Structure

The structure of an islanded microgrid is shown in Fig. 1. The microgrid considered in this paper operates at the low-voltage power distribution level (208 V_{l-l}). Each DG unit is connected to the microgrid bus through a feeder. The loads connected to the microgrid bus are lumped into a single load. The focus in this paper is on the fundamental real and reactive power sharing, as in [24] and [28], and therefore only linear loads are considered. Each DG unit consists of a primary energy source, a three-phase inverter, and an *LC* filter. The feeder impedance includes the impedances of the interface inductor, isolation transformer, and the impedance of the feeder cables.

The local controllers can communicate information, such as real power and reactive power measured at the DG unit output, to the central energy management system (EMS) over a communication link. Since the proposed strategy only requires that the local controllers exchange data periodically at a slow rate, low-bandwidth communication links are considered adequate for this application. The local controller consists of the power

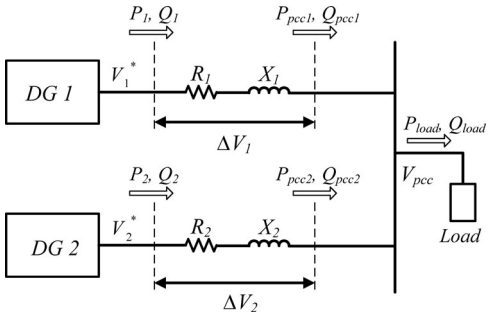

Fig. 2. Simplified model of the microgrid with two inverters.

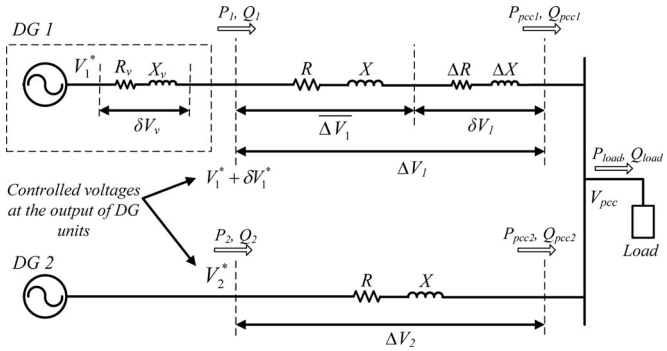

Fig. 3. Detailed network model as seen from *DG 1*.

controller, which generates the output voltage reference, and the voltage controller to track the voltage reference. Conventional frequency and voltage droop control is implemented in the controller as follows:

$$\omega = \omega_o - mP_m \tag{1}$$

$$V^* = V_o - nQ_m \tag{2}$$

where ω and V^* are the frequency and voltage magnitude references, respectively. P_m and Q_m are the real and reactive powers measured at the output of the DG unit, respectively, and are filtered to extract the fundamental power components. m is the frequency droop coefficient and n is the voltage droop coefficient. It is worth mentioning that to facilitate the utilization of the droop control concept in low-voltage distribution networks, a physical and/or a virtual interface inductor is commonly added in line at the output of the DG unit in an attempt to reduce the coupling between the real and the reactive power flows.

B. Reactive Power Sharing Analysis

The effect of the feeder impedance mismatch on the reactive power sharing is examined in this section by analyzing the voltage drop across the feeders. The voltage drop across the feeder impedance can be approximated as in [24] and [21]

$$\Delta V \approx \frac{XQ + RP}{V_o} \tag{3}$$

where X and R represent the feeder reactance and resistance, P and Q represent the real and reactive power flowing through the feeder, respectively, and V_o is the DG unit nominal output voltage. Without loss of generality, a two unit microgrid as shown in Fig. 2 is used as a case study in this section. The voltage drops across Feeder 1 and Feeder 2 in Fig. 2 can be approximated by

$$\Delta V_1 \approx \frac{X_1 Q_1 + R_1 P_1}{V_o} \tag{4}$$

$$\Delta V_2 \approx \frac{X_2 Q_2 + R_2 P_2}{V_o}. \tag{5}$$

The mismatch in the feeder impedances is given by

$$\Delta X = X_1 - X_2 \tag{6}$$

$$\Delta R = R_1 - R_2. \tag{7}$$

Considering (6) and (7), the network as seen from *DG 1* is shown in Fig. 3, where V_1^* and V_2^* represent the voltage references generated by the conventional droop controllers. X and R are the reactance and resistance of Feeder 2 (X_2 and R_2), respectively, that are chosen as references to calculate the mismatch between feeder impedances. X_v and R_v stand for the effect of any virtual impedance that might be implemented in the controller. δV_1^* represents the net change in the voltage reference that could be added by the controller, as will be seen later, to enhance the performance of the conventional droop control. Note that with proper design of the voltage controller, the voltages controlled and measured at the output filter capacitors of the DG units are assumed to match the references $V_1^* + \delta V_1^*$ and V_2^* at the steady state. P_1, Q_1, P_2, and Q_2 are the powers that can be measured at the outputs of the DG units. Based on Fig. 3 and (3)

$$\begin{aligned}\Delta V_1 &\approx \frac{(X + \Delta X)Q_1 + (R + \Delta R)P_1}{V_o} \\ &= \frac{XQ_1 + RP_1}{V_o} + \frac{\Delta XQ_1 + \Delta RP_1}{V_o} \\ &= \overline{\Delta V_1} + \delta V_1\end{aligned} \tag{8}$$

where as shown in Fig. 3, ΔV_1 is the total voltage drop across the Feeder 1 impedance represented by $X + \Delta X$ and $R + \Delta R$. $\overline{\Delta V_1}$ is the voltage drop across Feeder 1 due to the reference reactance and resistance, X and R. δV_1 indicates the voltage drop mismatch between Feeder 1 and Feeder 2 due to the mismatch in feeder impedances, ΔX and ΔR. This voltage will cause unequal reactive power sharing between the DG units [16], [21], [22], [24]. One solution to this problem is to match the feeder impedances by using a virtual impedance of $X_v = -\Delta X$ and $R_v = -\Delta R$, which would result in $Q_{\mathrm{pcc1}} = Q_{\mathrm{pcc2}}$. It is important to mention that if the DG units have different ratings then the feeder reactance and resistance must be modified to be inversely proportional to the Q and P ratings, respectively, in order to achieve proper proportional reactive power sharing [16], [25], [26]. The drawback of this technique is that it requires knowledge of the feeder impedances which is often not readily available.

The other way to resolve this issue, as proposed in this paper, is to employ voltage drop compensation instead of matching impedances. Without loss of generality, the case where both units have the same rating is considered in this analysis.

When using conventional droop control only, V_1^* and V_2^* can be represented as

$$V_1^* = V_{\rm pcc} + \overline{\Delta V_1} + \delta V_1 \tag{9}$$

$$V_2^* = V_{\rm pcc} + \Delta V_2. \tag{10}$$

The effect of the voltage drop mismatch due to ΔX and ΔR on reactive power sharing can be compensated by modifying the voltage reference V_1^* as follows:

$$V_1^* + \delta V_1^* = V_{\rm pcc} + \overline{\Delta V_1} + \delta V_1 \tag{11}$$

assuming that a controller can be designed such that at any time

$$\delta V_1^* = \delta V_1. \tag{12}$$

Consequently, (11) can be reduced to

$$V_1^* = V_{\rm pcc} + \overline{\Delta V_1}. \tag{13}$$

Although ΔV_1 will still not be equal to ΔV_2, the effect of δV_1 on the reactive power sharing will be compensated. For example, every time δV_1 increases due to an increase in load, the controller will increase δV_1^* accordingly. This can be implemented by using an adaptive virtual impedance and communication as proposed in the next section.

III. Proposed Control Strategy

A. Proposed Controller

The feasibility of the condition in (12) can be further investigated by using the principle of virtual impedance and the approximation in (3). Considering the use of a virtual impedance to generate the voltage δV_1^*, from Fig. 3

$$-\delta V_v = \delta V_1^*. \tag{14}$$

Using the approximation in (3), the condition in (12) can be approximated by

$$-\frac{X_v Q_1 + R_v P_1}{V_o} \approx \frac{\Delta X Q_1 + \Delta R P_1}{V_o}. \tag{15}$$

Satisfying (15) by matching the impedances is not practical as stated in Section II. However, (15) can be simplified by setting

$$\tilde{K}_v = X_v = R_v \tag{16}$$

where $\tilde{K}_v$ is called the virtual impedance variable. The condition in (16) will result in a feasible controller as will be shown later in this section. Substituting (16) in (15) and rearranging

$$\tilde{K}_v \approx -\frac{\Delta X Q_1 + \Delta R P_1}{Q_1 + P_1}. \tag{17}$$

As can be seen from (17), for any given values of ΔX, ΔR, P_1, and Q_1, there is a corresponding $\tilde{K}_v$ that matches the voltages to meet the condition in (12). However, (17) still cannot be used to implement the controller because the feeder discrepancies (ΔX and ΔR) are unknown. Nevertheless, the main goal of (17) is to show that one value for the virtual reactance and resistance can satisfy the condition in (12).

If the proper reference for Q_1 is available to the local controller, the variable $\tilde{K}_v$ can be tuned to the required virtual impedance value as proposed in this paper. To achieve this, each unit shares its actual reactive power load with the microgrid EMS over the communication link. The EMS calculates the proper share for each unit based on its rating and the total load and sends it back to each unit, along with a controller enable signal (EN). Note that the communication link is not used here within the closed loop of the tuning control, but instead it is used to set the reactive power reference that will be used in the tuning process. Therefore, the sharing accuracy at steady state is unaffected by time delays in the communication channels.

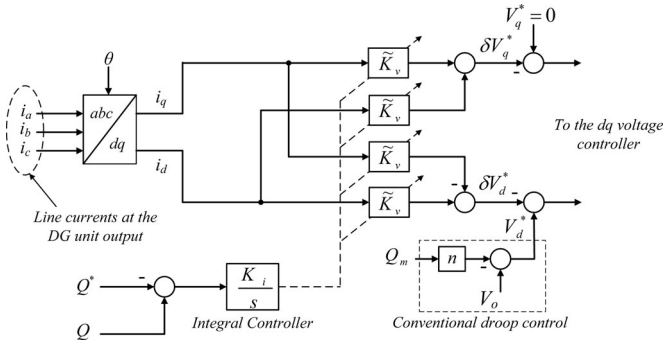

Fig. 4. Proposed adaptive virtual impedance controller.

Consequently, each unit will utilize the received reactive power share reference Q^* to adaptively tune $\tilde{K}_v$. The received Q^* value will not vary with transients in the reactive power of each unit caused by the tuning process, since it is calculated based on the total reactive power load. Therefore, Q^* will be a fixed reference until the total reactive power load changes.

Once $\tilde{K}_v$ is tuned for a given load condition, accurate reactive power sharing will continue even if the communication channel becomes unavailable, as long as the load does not change. Even if the load changes while communication is disrupted, there will be a smaller sharing error in comparison to the conventional droop control case, as will be shown in Sections IV and V.

The proposed controller to tune the virtual impedance variable $\tilde{K}_v$ is shown in Fig. 4. A simple integral control loop can be used to tune $\tilde{K}_v$ by regulating Q indirectly to match Q^*. The virtual impedance is implemented in the dq-frame where θ represents the phase angle of the unit output voltage. Note that the objective of the controller is not to regulate the reactive power directly but to tune the virtual impedance to a value that compensates for the effect of the feeder mismatch on the reactive power sharing. Therefore, once the virtual impedance is tuned for the current load conditions it will result in accurate sharing, and in reasonable sharing if the load changes and communication is disrupted. More details regarding the communication loss and delay will be discussed in Sections III-C, IV, and V.

For a microgrid of two DG units, the controller can be implemented in one unit only or in both units. A similar analysis to that presented in Section II-B can be developed for *DG 2* considering that the network seen by the second unit can be represented similarly to that in Fig. 3. In general, for a microgrid with two or more DG units, the controller implemented at each unit tunes the virtual impedance in the same way as described previously for *DG 1*.

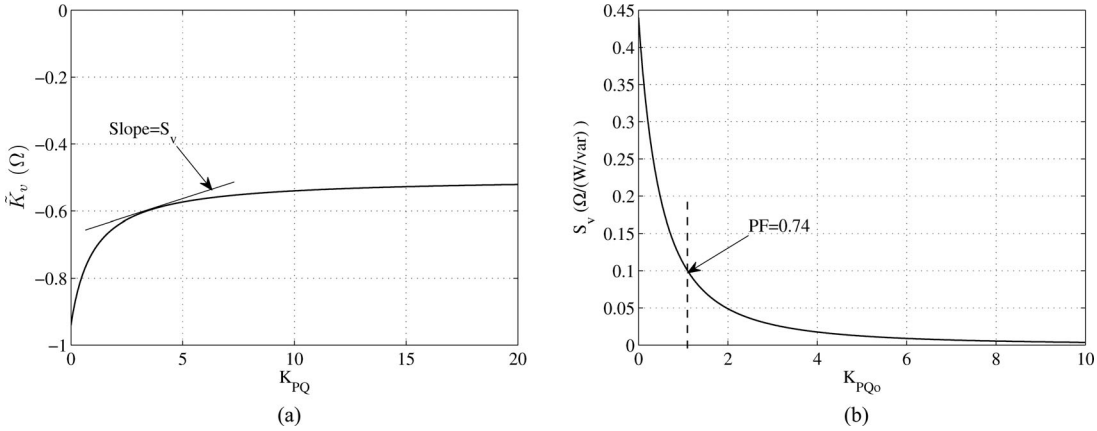

Fig. 5. $\tilde{K}_v$ sensitivity based on the parameters of DG units 1 and 2 from Table I ($\Delta X = 0.94\ \Omega$, $\Delta R = 0.5\ \Omega$). (a) $\tilde{K}_v$ as a function of the load operating point. (b) S_v in the considered operating range.

TABLE 1
SYSTEM PARAMETERS

Description	Parameter	Value
DG Unit Rating	S	1 kVA
Nominal Voltage	V_o	208 V_{l-l}
Inverters Filter	L_f, C_f	5mH, 75μF
Switching Frequency	f_s	10 kHz
Frequency Droop Coefficient	m	0.00105 rad/(s·W)
Voltage Droop Coefficient	n	0.00250 V/var
Feeder 1 Impedance	$R_1 + jX_1$	$1.6 + j2.450\ \Omega$
Feeder 2 Impedance	$R_2 + jX_2$	$1.1 + j1.508\ \Omega$
Feeder 3 Impedance (simulation)	$R_3 + jX_3$	$0.8 + j1.130\ \Omega$
Total Load (simulation)	P_L, Q_L	1215 W, 1030 var
Total Load (experimental)	P_L, Q_L	1170 W, 1330 var
Q^* setpoint update rate	f_c	5 Hz
Integral Control gain	K_i	0.005 Ω/(s·var)
LPF Time Constant	T	0.016 rad/s

The integral control is chosen such that the integration time is much longer than the information update period, e.g., the integration time $T_i = 1/K_i$ is chosen to be 200 s·var/Ω, versus an information update period of 0.2 s (see Table I). Therefore, the time delay in the received Q^* sample, due to the fact that reference Q^* is updated periodically, will have no effect on the reactive power sharing at steady state. This time delay is called the information update delay. Moreover, the tuning loop is slow enough that the interaction is negligible with the microgrid dynamics, which are dominated by the power low-pass filter dynamics [31], [32]. A detailed small-signal model of the virtual impedance tuning loop is developed and presented in the Appendix.

Note that the reference Q^* is calculated by the EMS based on the total reactive power load in the microgrid, therefore Q^* stays unchanged during the tuning action unless the total load changes. This part of the strategy can be considered to be a supervisory control system, which reacts only when the total load in the microgrid changes (a disturbance).

B. Tuned Controller Sensitivity to Operating Points

The proposed controller is designed so that the tuned virtual impedance is held at its most recent value after a communication failure occurs, as will be illustrated in the following section. If the operating point remains unchanged after the communication failure, the sharing error will remain zero since the controller is already tuned for that operating point. However, an operating point change will result in a sharing error because $\tilde{K}_v$ can no longer adapt to the new operating point. The change needed in $\tilde{K}_v$ to adapt to the new operating point defines the sensitivity of $\tilde{K}_v$ with respect to the change in the operating point. To gain insight into the $\tilde{K}_v$ sensitivity, the approximated relation in (17) is used. Rearranging the terms in (17)

$$\tilde{K}_v \approx -\frac{\Delta X + \Delta R(P/Q)}{1 + (P/Q)}. \tag{18}$$

It is clear from (18) that $\tilde{K}_v$ depends on the ratio P/Q rather than on the value of P or Q separately. Therefore, any new operating point with the same ratio P/Q (the same power factor) will result in the same $\tilde{K}_v$. Define the variable K_{PQ} as P/Q. The nonlinear relation in (18) can be linearized around the operating point as follows:

$$\tilde{K}_v \approx \tilde{K}_{vo} + \frac{\partial \tilde{K}_v}{\partial K_{PQ}}\Big|_{K_{PQo}} \Delta K_{PQ} \tag{19}$$

where $\tilde{K}_{vo}$ is the virtual impedance variable tuned at the operating point and K_{PQo} is the associated P/Q ratio. The slope of $\tilde{K}_v$ in (19) is defined as the sensitivity S_v around the operating point. Therefore, S_v can be written as

$$\begin{aligned} S_v &= \frac{-\partial}{\partial K_{PQ}} \left(\frac{\Delta X + \Delta R K_{PQ}}{1 + K_{PQ}} \right) \Big|_{K_{PQo}} \\ &= \frac{-(1 + K_{PQo})\Delta R + (\Delta X + \Delta R K_{PQo})}{(1 + K_{PQo})^2}. \end{aligned} \tag{20}$$

To gain insight into the sensitivity of $\tilde{K}_v$ to the operating point, feeders 1 and 2 from Table I are considered, where $\Delta X = 0.94\ \Omega$ and $\Delta R = 0.5\ \Omega$. As can be seen from Fig. 5(a) and (18) when K_{PQ} is zero (PF = 0) then $\tilde{K}_v$ equals $-\Delta X$. However, when K_{PQ} approaches infinity (PF = 1) $\tilde{K}_v$ equals $-\Delta R$. Consequently, for high K_{PQ} values (high power factors) the sensitivity of $\tilde{K}_v$ is low as shown in Fig. 5(b). From Fig. 5(b), $|S_v|$ is less than 0.1 for power factors higher than 0.74 and $\tilde{K}_v$

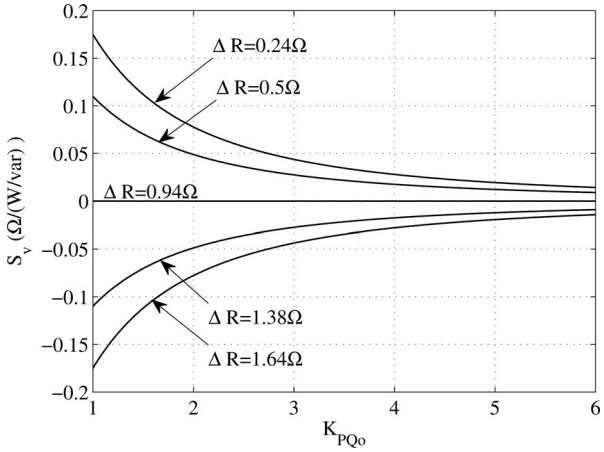

Fig. 6. Sensitivity of $\tilde{K}_v$ for different values of ΔR ($\Delta X = 0.94\ \Omega$).

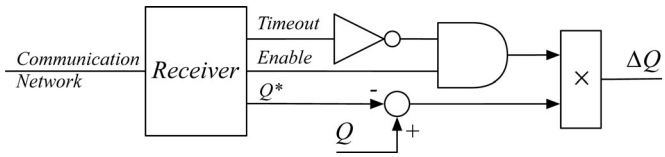

Fig. 7. Reactive power setpoint enable logic in each local controller.

changes from $-0.646\ \Omega$ to $-0.521\ \Omega$ when K_{PQ} changes from 2 (PF = 0.89) to 20 (PF = 0.998). To examine the effect of different impedance pairs, ΔX is fixed at 0.94 Ω and ΔR is changed as shown in Fig. 6. Again, Fig. 6 shows low sensitivity for high K_{PQ} (high PF), e.g., $|S_v|$ is less than 0.1 for K_{PQ} higher than 1.65 (PF = 0.85).

C. Information Management Structure

The EMS periodically polls the inverters for their internally measured reactive power output. The update rate for the reactive power data can be chosen based on the specifications of the available communication link. The collected reactive power measurements are then summed and weighted such that each inverter is responsible for sharing the reactive power in proportion to its rating. The resulting values are then passed back to the inverters as setpoints for the tuning control loop.

The receiver is capable of detecting a communication time out, in which case the control loop is disabled and the integrator output will remain constant until a valid setpoint is again received. The timeout/enable logic is shown in Fig. 7. Note that when the EMS detects a communication timeout from one DG unit it blocks further setpoint updates to all the DG units until communication is restored. Since the updates are not sent to the remaining DG units their timeout/enable logic disables the tuning control loops until communication is restored. A binary EN is also sent along with the setpoint to allow for remote enabling and disabling of the tuning control loop.

IV. Simulation Results

A microgrid with three DG units is simulated in the PSCAD/EMTDC environment to validate the proposed control strategy, and to demonstrate the feasibility of the proposed controller for microgrids with more than two units. The microgrid system parameters are shown in Table I. The three DG units are identical in rating and filter parameters to highlight the accuracy of the proposed strategy in the presence of mismatched feeder impedances. The discrepancy in the feeder impedances is chosen to be significant in comparison to values used in the existing literature [23], [24], [28].

To evaluate the performance of the proposed system a percentage accuracy measure Q_{er} is defined as in [28]

$$Q_{er,i}\% = \frac{Q_i - Q_i^*}{Q_i^*} \times 100 \tag{21}$$

where Q_i is the reactive power measured at the output of unit i and Q_i^* is the desired reactive power share of unit i. Simulation scenarios that validate the performance of the proposed controller are presented in the following sections.

1) Performance of Conventional Controller: The performance of the system using only conventional droop control is illustrated in Fig. 8 for two different loads. The total reactive power load is changed between 1030 and 388 var while the real power load is changed between 1215 and 910 W. These load settings represent a larger change in reactive power load as compared to the change in the real power load to show the low sensitivity of the tuned virtual impedance to the P/Q ratio factor (K_{PQ}) of the operating point as discussed in Section III-B. Also, this will help to evaluate the control strategy for a wide range of load power factors, from 0.76 for the higher load to 0.92 for the lower load.

From Fig. 8, the reactive power sharing accuracy under conventional droop control is as poor as 45 % for Unit 3 and 44% for Unit 1 while it is 2.9 % for Unit 2, calculated at the higher load operating point.

2) Performance of the Proposed Controller: The performance of the proposed controller is demonstrated in Fig. 9. The controller is enabled at $t = 1$ s which reduces the reactive power sharing error to zero in 2 s as can be seen in Fig. 9(b). Also, Fig. 9(a) shows that the controller action has only a small transient effect on the real power supplied by each unit. Moreover, Fig. 9(c) illustrates the low sensitivity of the tuned virtual impedances to a change in the operating point.

The behavior of the microgrid bus voltage $V_{\rm pcc}$, when the controller is enabled at $t = 1$ s, is shown in Fig. 10. As can be seen, the voltage drop introduced by the proposed controller is negligible (0.0015 pu). This is due to the fact that controllers reduce the total feeder impedance for the unit with the higher physical impedance (Unit 1), and increase it for the unit with the lower physical impedance (Units 2 and 3), as can be noticed from Fig. 9(c). The latter voltage change, when the load stepped down, is mainly due to the change in the voltage drop across the feeders and the conventional voltage droop action, since the virtual impedances did not change significantly [see Fig. 9(c)] when the load changed.

Fig. 11 demonstrates the enhancement in the current sharing accuracy provided by the proposed control strategy as compared to the conventional droop control.

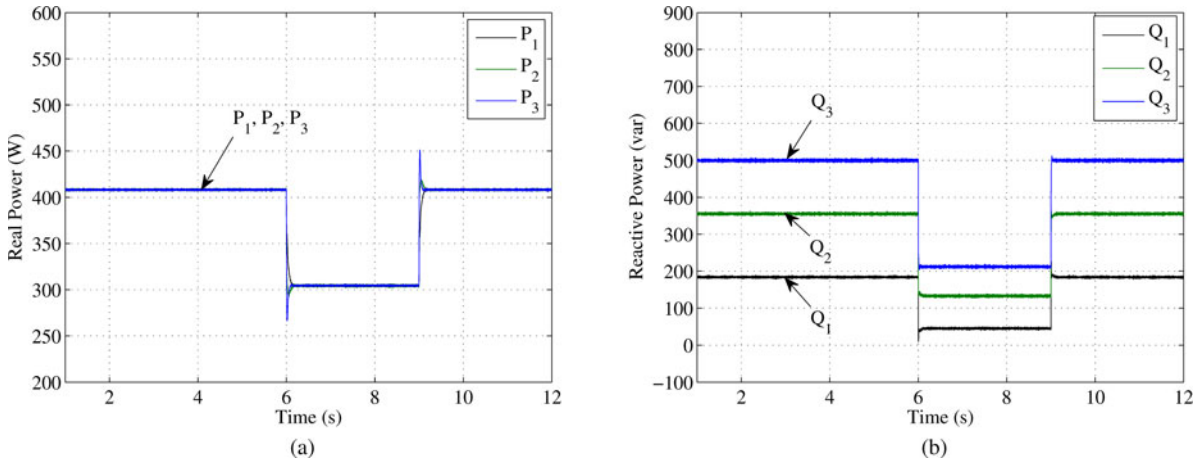

Fig. 8. Simulated performance of conventional droop control. (a) Real power. (b) Reactive power.

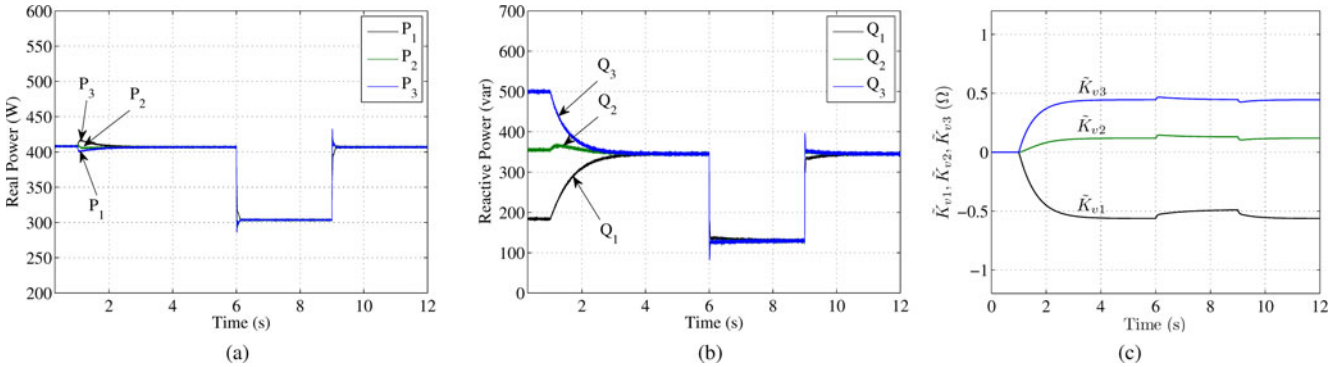

Fig. 9. Simulated performance of the proposed controller (activated at t = 1 s). (a) Real Power. (b) Reactive Power. (c) Real-time tuning of the virtual impedance variables.

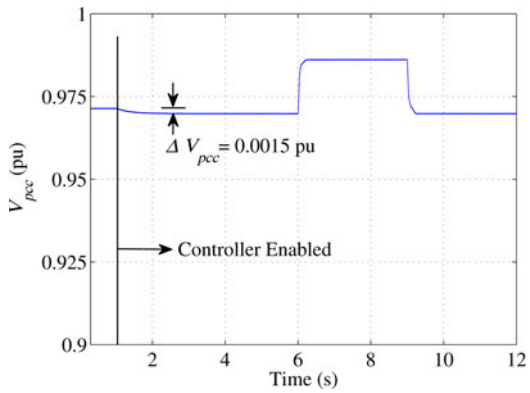

Fig. 10. Behavior of the microgrid bus voltage ($V_{\rm pcc}$) when the controller is enabled at $t = 1$ s.

3) Effect of the Communication and Information Update Delays: To show the main concept of the controller, two factors were neglected in the simulation of Fig. 9. The first is the time delay mismatch among the communication channels, and the second is the information update delay. In Fig. 9, the load is intentionally changed at the same moment Q^* is updated so there is no information update delay. A second simulation is performed to include these effects. A delay of 0.1 and 0.05 s has been included in the communication links of units 2 and 3, respectively, while no delay is considered for unit 1 to emphasize the delay time mismatch. Also, the load changes have been introduced exactly in the middle between the Q^* update times, which results in a 0.1 s information update delay. Note that the time delay is significant with respect to the 0.2 s update rate of Q^*. Taking into account these changes, the performance of the proposed control strategy is shown in Fig. 12. As can be seen the information update delay and the time delay mismatch has no effect on the sharing accuracy of the proposed controller. The same time delay in the communication channels will be used for the remainder of the simulation scenarios.

4) Controller Performance During a Communication Disruption: The scenario of a communication failure is illustrated in Fig. 13. A communication failure is sensed at $t = 5$ s causing a timeout signal issued by the serial receiver block (see Fig. 7) to disable the controller. The virtual impedance variables are held at the last value before the failure occurred due to the integral action of the controller. As can be seen in Fig. 13(a) when the load changes the sharing error is still acceptable. A noticeable change in the operating point power factor from 0.76 to 0.92 is considered here to give insight into the sensitivity of the virtual impedance to a change in the load. The sharing error accuracy ($Q_{er,i}\%$) is 6.2%, -1.87%, and 1.87% for DG units 1, 2, and 3, respectively, as compared to -46.8%, 2.92%, and 45.48% when using conventional droop control only.

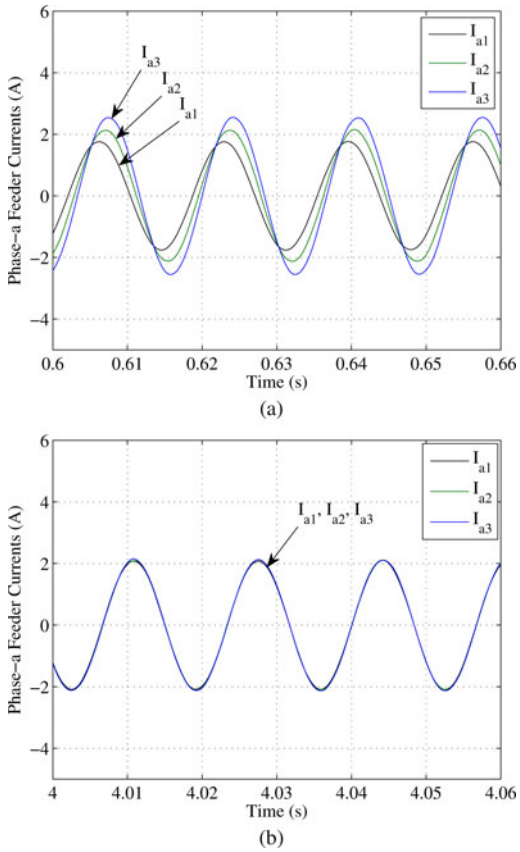

Fig. 11. Simulated feeder currents. (a) Under conventional control (before enabling the controller). (b) Under the proposed control strategy.

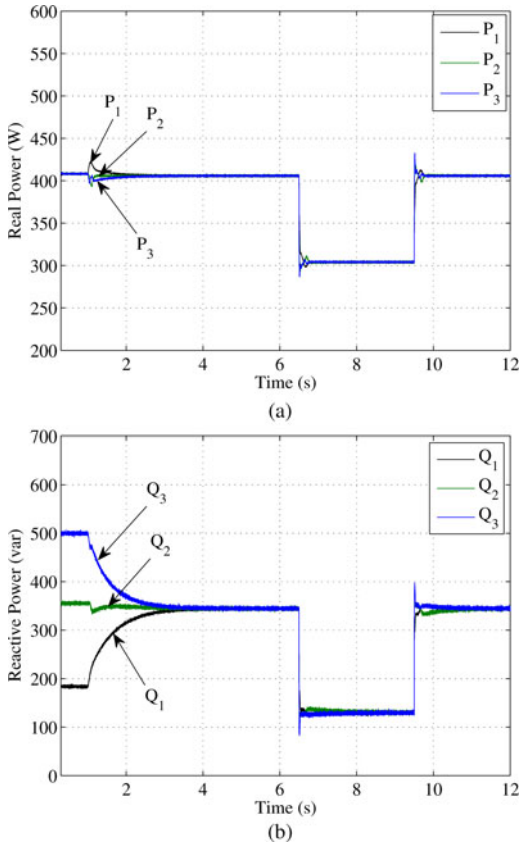

Fig. 12. Simulated performance of the controller considering the effects of time delay mismatches among the communication channels and the information update delay. (a) Real power. (b) Reactive Power.

Associated feeder current waveforms for the three DG units are shown in Fig. 13(b) which demonstrate accurate sharing compared to the current waveforms in Fig. 11(a). Finally, Fig. 14 shows the system transient performance during the restoration of communication at $t = 9$ s. The sharing mismatch is reduced once communication is restored.

V. Experimental Validation

A. Experimental Setup

The experimental setup consists of two three-phase inverters with Ethernet interfaces, a networked computer running the EMS software, and a load with adjustable real and reactive power levels. The primary power sources for the inverters are two Chroma 62050H power supplies. The inverters are based on Powerex PS22A78-E IGBT modules. Current and voltage sensing are implemented using LEM LA 20-PB and LV-20-P Hall effect sensors, respectively. Other experimental system parameters including the LC filter values and feeder impedances are shown in Table I for units 1 and 2.

The inverter controllers are implemented in Simulink, compiled using the Embedded Coder toolchain, and run on Spectrum Digital eZdsp boards containing Texas Instruments TMS320F28335 32-bit floating-point microcontrollers. The network interfaces are implemented with Texas Instruments serial-to-ethernet modules connected to the serial communication port of the eZdsp boards.

Each unit in the prototype microgrid is connected to the bus through a 3 mH interface inductor, an isolating transformer with a leakage inductance of 1 mH, and a resistance of 1.1 Ω. Moreover, an additional 2.5 mH (0.94 Ω) inductor and 0.5 Ω resistor are added in line with Unit 1 to generate the mismatch in the feeder impedances.

The EMS software that receives the measured reactive powers and calculates the reactive power setpoints is programmed in the Python language and hosted on a PC running Ubuntu Linux. A photograph of the experimental apparatus is shown in Fig. 15.

Two load operating points are considered to validate the proposed controller. At the high load point, $P_{\rm load}$ is chosen as 1170 W and $Q_{\rm load}$ as 1330 var which results in a PF of 0.66. At the low load point, $Q_{\rm load}$ is stepped down to 890 var while $P_{\rm load}$ is stepped down only by 32 W to 1136 W (PF = 0.79) to emphasize the change in P/Q ratio. Moreover, the power factor is deliberately chosen to be low at both operating points to validate the proposed controller in the lower power factor region where sensitivity S_v is higher as discussed in Section III-B.

B. Experimental Results

Experiments were performed to validate the effectiveness of the proposed controller. The results for a conventional controller,

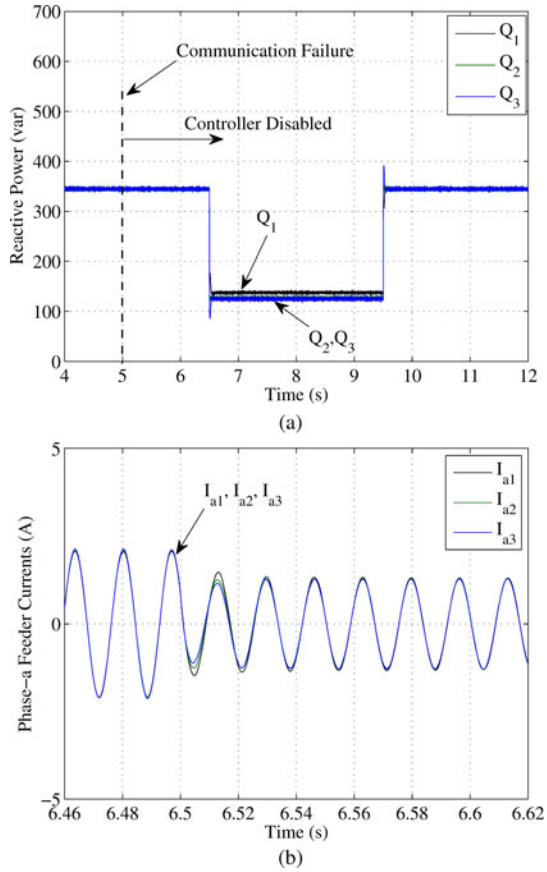

Fig. 13. Simulated performance of the tuned controller in response to a load change after a communication failure. (a) Reactive Power. (b) Phase-a feeder currents.

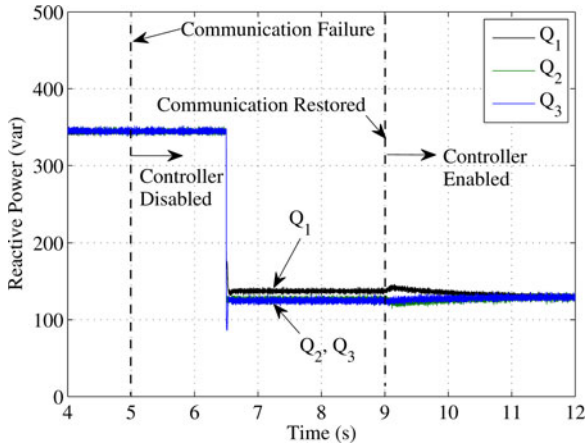

Fig. 14. Simulated system performance during communication restoration.

the proposed controller, and the enhanced controller in the presence of communication failures and time delays are presented and discussed.

The real power and reactive power are measured internally in the controller platform and are output as analog signals using PWM-DACs. The scaled *P* and *Q* values are then captured and displayed.

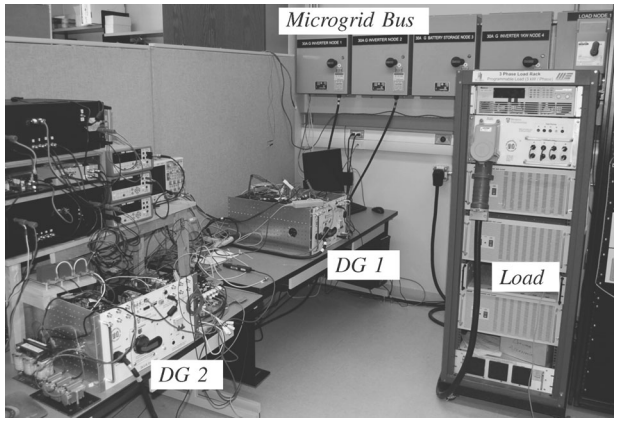

Fig. 15. Experimental apparatus.

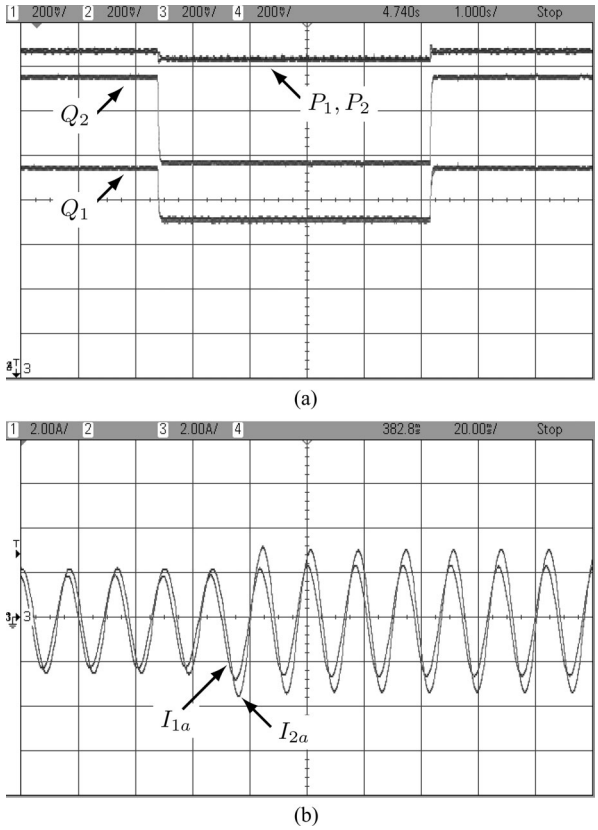

Fig. 16. Power and current sharing under conventional droop control. (a) Real and reactive power from each inverter with step changes in the load. P_1, P_2 start at 584 W and drop to 568 W; Q_1 starts at 498 var and drops to 298 var; Q_2 starts at 825 var and drops to 522 var. (Vert: 150 VA/div; Horiz: 1 s/div) (b) Phase-a currents from each inverter for two different load operating points. (Vert: 2 A/div; Horiz: 20 ms/div).

1) Performance of the Conventional Controller: In Fig. 16(a), the real and reactive powers from each inverter operating under a conventional droop control scheme are shown. While the droop mechanism ensures that the real power is shared evenly between the inverters, the different feeder impedances of the units result in reactive power being shared unevenly. At the higher reactive load, the sharing accuracy errors are $Q_{er,1} = -25\,\%$ and $Q_{er,2} = 25\,\%$.

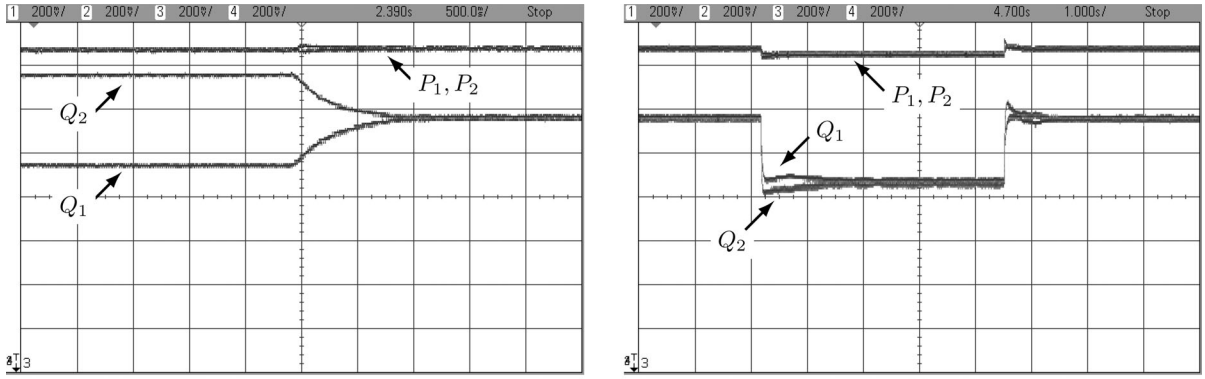

Fig. 17. Real and reactive power sharing. (Vert: 150 VA/div) (a) As the proposed control loop is enabled. P_1, P_2 are each 584 W. Q_1 and Q_2 are initially 498 and 825 var, respectively, and each converge to 665 var when the controller is enabled. (b) A step change in the load operating point with the controller enabled. The steady-state reactive power for each inverter steps from 665 to 445 var and back.

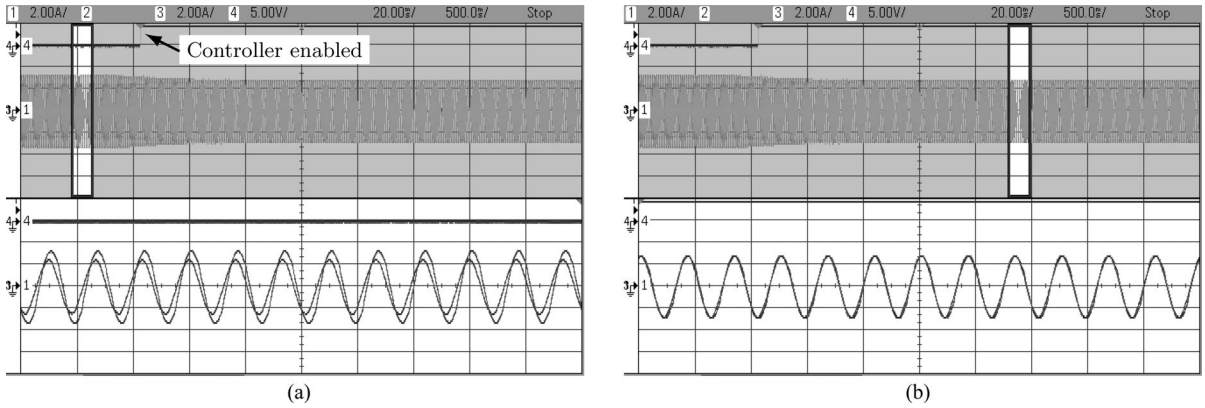

Fig. 18. Improvement in current sharing accuracy (phase-a). (a) Conventional controller (before enabling the proposed controller). (b) Proposed controller enabled. (Vert: 2 A/div; Horiz : upper 500 ms/div, lower 20 ms/div).

The currents are shown in Fig. 16(b) and clearly demonstrate the mismatch between the inverters. Each current is measured at the transformer secondary and therefore does not include the portion of the associated reactive power absorbed by the transformer, which is approximately 200 var.

2) Performance of the Proposed Controller: When the proposed controller is enabled the virtual impedances for the two inverters are adjusted so that they share $Q_{\rm load}$ evenly as shown in Fig. 17(a). The system behavior when there is a step change in the load power is shown in Fig. 17(b), demonstrating that the controller is effective at different load operating points. Immediately after the step there is a slight reactive power mismatch while the virtual impedances are adapted to the new operating point.

The currents before and after the enhanced control loop are enabled as shown in Figs. 18(a) and (b), respectively, and show accurate steady-state sharing after the controller is enabled.

3) Performance During a Communication Failure: Fig. 19 shows the reactive power from each inverter along with an active-high signal that indicates whether the enhanced controller is enabled. To create a realistic failure scenario, the Ethernet cable is unplugged from one of the DG units. The virtual impedance has adapted for the higher level of reactive power prior to the communication failure. When the Ethernet cable is unplugged the receive block detects the timeout and disables the control loop as shown in Fig. 7, thus holding $\tilde{K}_v$ at its last tuned value. When the reactive load drops this results in some mismatch between the shared Q due to the inactive enhanced control loop. The sharing accuracy errors are $Q_{er,1} = 4.0\,\%$ and $Q_{er,2} = -4.0\,\%$. When Q increases back to its original level

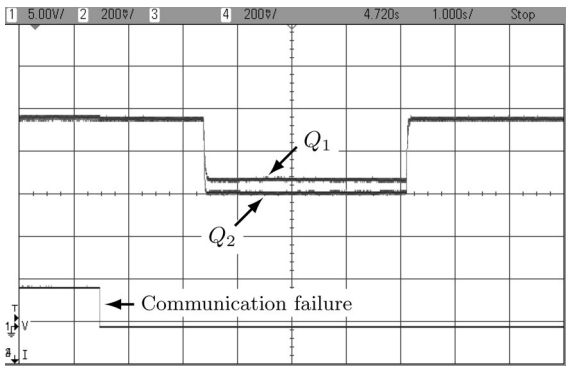

Fig. 19. Performance of the tuned controller in response to a load change after a communication failure. The lower trace shows the controller enable signal. Q_1, Q_2 are even at 665 var each and continue at this level after communication is lost. When the reactive load is changed Q_1 drops to 439 var and Q_2 drops to 405 var. (Vert: 150 var/div; Horiz: 1 s/div).

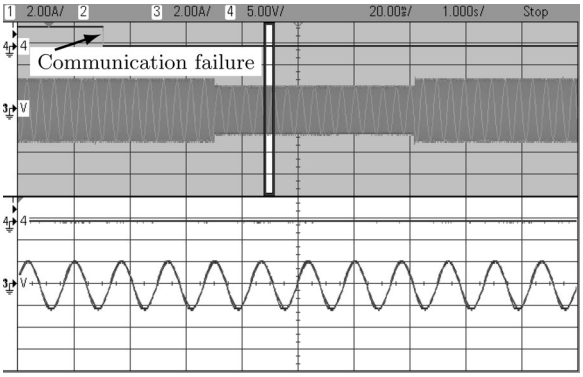

Fig. 20. Phase-a current sharing during a communication failure with a change in reactive power load. (Vert: 2 A/div; Horiz: upper 1 s/div, lower 20 ms/div).

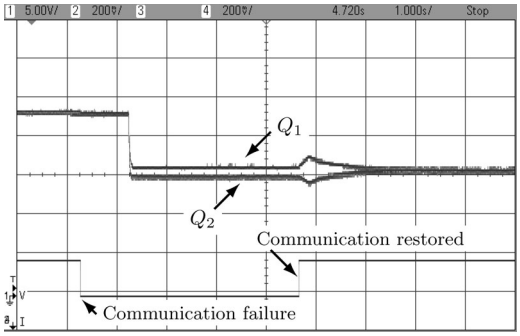

Fig. 21. Reactive power from each inverter when communication is lost and restored (upper traces). The lower trace shows the controller enable signal. (Vert: 150 var/div; Horiz: 1 s/div).

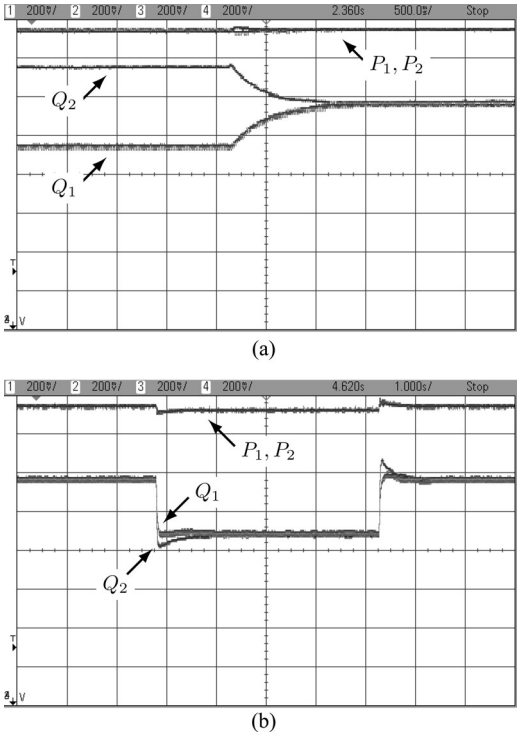

Fig. 22. Real and reactive power sharing with a time delay mismatch in the communication channels. (a) As the proposed control loop is enabled. (Vert: 150 var/div; Horiz: 500 ms/div) (b) A step change in the load with the controller enabled. (Vert: 150 var/div; Horiz: 1 s/div).

the reactive power is again shared accurately. Fig. 20 shows the phase-a current sharing during a communication failure with a change in reactive power load.

In Fig. 21, the effect of restoring communication is illustrated. When communication with the EMS is restored the enhanced controller is reenabled and the error between the two reactive power outputs is rolled up as the virtual impedance is adapted to the lower reactive power level.

4) Performance in the Presence of Delays in Communication: The effects of a delay of 0.1 s in the communication channel to *DG 1* and 0.05 s in the communication channel to *DG 2* are shown in Figs. 22(a) and (b). As can be seen, the time delay does not affect the sharing accuracy and the difference in the transient behavior is negligible in comparison to the case shown in Fig. 17(a).

VI. Conclusion

A control strategy to improve reactive power sharing in an islanded microgrid has been proposed and validated in this paper. The strategy employs communication to exchange the information needed to tune adaptive virtual impedances in order to compensate for the mismatch in feeder impedances. The control strategy does not require knowledge of the feeder impedances, and is straightforward to implement in practice. It is also insensitive to time delays in the communication channels. It has been shown that the proposed technique is tolerant of disruptions in the communication links while still outperforming the conventional droop control method. The sensitivity of the tuned controller parameters to changes in the system operating point has also been investigated. It has been shown that the system operating point is mainly determined by the power factor, and the higher the load power factor, the less sensitive the parameters are to the operating point. The control strategy has been simulated and implemented in a 2-kVA experimental system and has been verified to be effective under operating point changes and realistic communication failures.

Appendix
Small-Signal Model of the Virtual Impedance Tuning Loop

The real and reactive power flow can be described as in [33]

$$P = \frac{1}{R_t^2 + X_t^2}(R_t V^{*2} - R_t V^* V_{\rm pcc}\cos\delta + X_t V^* V_{\rm pcc}\sin\delta) \tag{22}$$

$$Q = \frac{1}{R_t^2 + X_t^2}(X_t V^{*2} - X_t V^* V_{\rm pcc}\cos\delta - R_t V^* V_{\rm pcc}\sin\delta) \tag{23}$$

where the angle δ is the power angle. R_t and X_t represent the resistive and inductive components of the total feeder impedance, respectively, including the virtual impedances as follows:

$$R_t = R + \tilde{K}_v \tag{24}$$

$$X_t = X + \tilde{K}_v \tag{25}$$

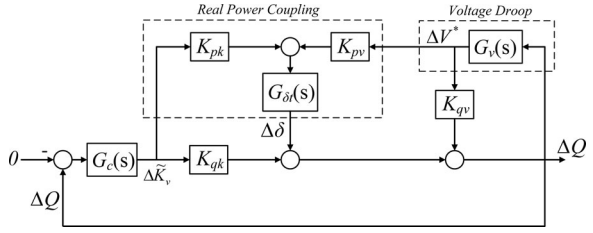

Fig. 23. Linearized model.

where $\tilde{K}_v$ is the virtual impedance variable generated by the controller as

$$\tilde{K}_v = \frac{K_i}{s}(Q - Q^*). \tag{26}$$

Linearizing (22), (23), (26), along with the frequency and voltage droop (1) and (2), around an operating point

$$\begin{aligned}\Delta P &= \left(\frac{\partial P}{\partial V^*}\right)\Delta V^* + \left(\frac{\partial P}{\partial \delta}\right)\Delta\delta + \left(\frac{\partial P}{\partial \tilde{K}_v}\right)\Delta\tilde{K}_v \\ &= K_{pv}\Delta V^* + K_{p\delta}\Delta\delta + K_{pk}\Delta\tilde{K}_v \end{aligned} \tag{27}$$

$$\begin{aligned}\Delta Q &= \left(\frac{\partial Q}{\partial V^*}\right)\Delta V^* + \left(\frac{\partial Q}{\partial \delta}\right)\Delta\delta + \left(\frac{\partial Q}{\partial \tilde{K}_v}\right)\Delta\tilde{K}_v \\ &= K_{qv}\Delta V^* + K_{q\delta}\Delta\delta + K_{qk}\Delta\tilde{K}_v \end{aligned} \tag{28}$$

$$\Delta\tilde{K}_v = \frac{K_i}{s}\Delta Q = G_c(s)\Delta Q \tag{29}$$

$$\Delta\omega = \frac{-m}{Ts+1}\Delta P \tag{30}$$

$$\Delta V^* = \frac{-n}{Ts+1}\,\Delta Q = G_v(s)\Delta Q \tag{31}$$

where K_{pv}, $K_{p\delta}$, K_{pk}, K_{qv}, $K_{q\delta}$, K_{qk} are calculated around the operating point, and T is the time constant of the low-pass filter used in the P and Q measurement channels. Considering that $\Delta\omega = s\Delta\delta$, (30) can be rewritten as

$$\Delta\delta = \frac{-m}{s(Ts+1)}\Delta P = G_\delta(s)\Delta P. \tag{32}$$

Substituting for ΔP from (32) in (27), $\Delta\delta$ is given by

$$\Delta\delta = G_{\delta t}(s)[K_{pv}\Delta V^* + K_{pk}\Delta\tilde{K}_v] \tag{33}$$

where

$$G_{\delta t}(s) = \frac{G_\delta(s)}{1 - K_{p\delta}G_\delta(s)}. \tag{34}$$

Equation (33) represents the coupling of the reactive power controller with the real power control dynamics. Using (28), (29), and (33), a block diagram of the system with the proposed controller can be realized as in Fig. 23. This model can be further simplified as in Fig. 24. Accordingly, the characteristic equation of the system is given by

$$\begin{aligned}&1 - K_{qv}G_v(s) - K_{pv}G_v(s)G_{\delta t}(s) - K_{qk}G_c(s) \\ &- K_{pk}G_c(s)G_{\delta t}(s) = 0. \end{aligned} \tag{35}$$

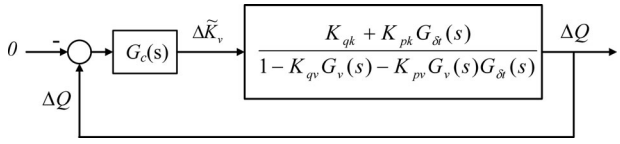

Fig. 24. Simplified block diagram of the linearized model.

Substituting for $G_c(s)$, $G_v(s)$, $G_\delta(s)$, and $G_{\delta t}(s)$ from (29), (31), (32), and (34), respectively, the characteristic equation is given as

$$a_4 s^4 + a_3 s^3 + a_2 s^2 + a_1 s + a_0 = 0 \tag{36}$$

where

$$a_4 = T^2 \tag{37}$$

$$a_3 = 2T + nK_{qv}T - K_{qk}K_iT^2 \tag{38}$$

$$a_2 = 1 + mK_{p\delta}T + nK_{qv} - 2K_{qk}K_iT \tag{39}$$

$$\begin{aligned}a_1 = {} & mK_{p\delta} + nmK_{qv}K_{p\delta} - nmK_{pv} \\ & - K_{qk}K_i(1 + mK_{p\delta}T) + K_{p\delta}K_imT \end{aligned} \tag{40}$$

$$a_0 = -K_{qk}K_imK_{p\delta} + K_{pk}K_im. \tag{41}$$

The characteristic equation (36) is used to calculate the poles of the system around the considered operating points for different values of K_i. Consequently, the integral gain K_i is chosen so that the dominant poles result in much slower dynamics in comparison to the reference Q^* update rate. Therefore, time delays in communication have a minor effect on the system transients when the total reactive load changes significantly (see Section III-A).

REFERENCES

[1] M. A. Zamani, T. S. Sidhu, and A. Yazdani, "Investigations into the control and protection of an existing distribution network to operate as a microgrid: A case study," *IEEE Trans. Ind. Electron.*, vol. 61, no. 4, pp. 1904–1915, Apr. 2014.

[2] J. A. P. Lopes, C. L. Moreira, and A. G. Madureira, "Defining control strategies for microgrids islanded operation," *IEEE Trans. Power Syst.*, vol. 21, no. 2, pp. 916–924, May 2006.

[3] R. H. Lasseter, J. H. Eto, B. Schenkman, J. Stevens, H. Vollkommer, D. Klapp, E. Linton, H. Hurtado, and J. Roy, "CERTS microgrid laboratory test bed," *IEEE Trans. Power Del.*, vol. 26, no. 1, pp. 325–332, Jan. 2011.

[4] C. N. Rowe, T. J. Summers, R. E. Betz, D. J. Cornforth, and T. G. Moore, "Arctan power–frequency droop for improved microgrid stability," *IEEE Trans. Power Electron.*, vol. 28, no. 8, pp. 3747–3759, Aug. 2013.

[5] K. De Brabandere, B. Bolsens, J. Van den Keybus, A. Woyte, J. Driesen, and R. Belmans, "A voltage and frequency droop control method for parallel inverters," *IEEE Trans. Power Electron.*, vol. 22, no. 4, pp. 1107–1115, Jul. 2007.

[6] M. Savaghebi, A. Jalilian, J. C. Vasquez, and J. M. Guerrero, "Autonomous voltage unbalance compensation in an islanded droop-controlled microgrid," *IEEE Trans. Ind. Electron.*, vol. 60, no. 4, pp. 1390–1402, Apr. 2013.

[7] I. U. Nutkani, P. C. Loh, and F. Blaabjerg, "Droop scheme with considering of operating cost," *IEEE Trans. Power Electron.*, vol. 29, no. 3, pp. 1047–1052, Mar. 2014.

[8] D. De and V. Ramanarayanan, "Decentralized parallel operation of inverters sharing unbalanced and nonlinear loads," *IEEE Trans. Power Electron.*, vol. 25, no. 12, pp. 3015–3025, Dec. 2010.

[9] J. M. Guerrero, M. Chandorkar, T.-L. Lee, and P. C. Loh, "Advanced control architecture for intelligent microgrids—Part I: Decentralized and

hierarchical control," *IEEE Trans. Power Electron.*, vol. 60, no. 4, pp. 1254–1262, Apr. 2013.
[10] J. M. Guerrero, J. C. Vasquez, J. Matas, L. G. de Vicuña, and M. Castilla, "Hierarchical control of droop-controlled ac and dc microgrids—A general approach towards standardization," *IEEE Trans. Ind. Electron.*, vol. 58, no. 1, pp. 158–172, Jan. 2011.
[11] M. N. Marwali, J.-W. Jung, and A. Keyhani, "Control of distributed generation systems—Part II: Load sharing control," *IEEE Trans. Power Electron.*, vol. 19, no. 6, pp. 1551–1561, Nov. 2004.
[12] J. C. Vasquez, J. M. Guerrero, M. Savaghebi, J. Eloy-Garcia, and R. Teodorescu, "Modeling, analysis, and design of stationary-reference-frame droop-controlled parallel three-phase voltage source inverters," *IEEE Trans. Ind. Electron.*, vol. 60, no. 4, pp. 1271–1280, Apr. 2013.
[13] M. Savaghebi, A. Jalilian, J. C. Vasquez, and J. M. Guerrero, "Secondary control scheme for voltage unbalanced compensation in an islanded droop-controlled microgrid," *IEEE Trans. Smart Grid*, vol. 3, no. 2, pp. 797–807, Jun. 2012.
[14] M Savaghebi, A. Jalilian, J. C. Vasquez, and J. M. Guerrero, "Secondary control for voltage quality enhancement in microgrids," *IEEE Trans. Smart Grid*, vol. 3, no. 4, pp. 1893–1902, Dec. 2012.
[15] M. A. Abusara, J. M. Guerrero, and S. M. Sharkh, "Line-interactive ups for microgrids," *IEEE Trans. Ind. Electron.*, vol. 61, no. 3, pp. 1292–1300, Mar. 2014.
[16] J. Kim, J. M. Guerrero, P. Rodriguez, R. Teodorescu, and K. Nam, "Mode adaptive droop control with virtual output impedances for an inverter-based flexible AC microgrid," *IEEE Trans. Power Electron.*, vol. 26, no. 3, pp. 689–701, Mar. 2011.
[17] W. Yao, M. Chen, J. Matas, J. M. Guerrero, and Z.-M. Qian, "Design and analysis of the droop control method for parallel inverters considering the impact of the complex impedance on the power sharing," *IEEE Trans. Ind. Electron.*, vol. 58, no. 2, pp. 576–588, Feb. 2011.
[18] J. M. Guerrero, J. Matas, L. G. de Vicuña, M. Castilla, and J. Miret, "Decentralized control for parallel operation of distributed generation inverters using resistive impedance," *IEEE Trans. Ind. Electron.*, vol. 54, no. 2, pp. 994–1004, Apr. 2007.
[19] J. M. Guerrero, L. G. de Vicuña, J. Matas, M. Castilla, and J. Miret, "Output impedance design of parallel-connected UPS inverters with wireless load-sharing control," *IEEE Trans. Ind. Electron.*, vol. 52, no. 4, pp. 1126–1135, Aug. 2005.
[20] A. Tuladhar, H. Jin, T. Unger, and K. Mauch, "Control of parallel inverters in distributed AC power systems with consideration of line impedance effect," *IEEE Trans. Ind. Appl.*, vol. 36, no. 1, pp. 131–138, Jan./Feb. 2000.
[21] Y. W. Li and C.-N. Kao, "An accurate power control strategy for power-electronics-interfaced distributed generation units operating in a low-voltage multibus microgrid," *IEEE Trans. Power Electron.*, vol. 24, no. 12, pp. 2977–2988, Dec. 2009.
[22] Q.-C. Zhong, "Robust droop controller for accurate proportional load sharing among inverters operated in parallel," *IEEE Trans. Ind. Electron.*, vol. 60, no. 4, pp. 1281–1290, Apr. 2013.
[23] X. Yu, A. M. Khambadkone, H. Wang, and S. T. S. Terence, "Control of parallel-connected power converters for low-voltage microgrid—Part I: A hybrid control architecture," *IEEE Trans. Power Electron.*, vol. 25, no. 12, pp. 2962–2970, Dec. 2010.
[24] J. He and Y. W. Li, "An enhanced microgrid load demand sharing strategy," *IEEE Trans. Power Electron.*, vol. 27, no. 9, pp. 3984–3995, Sep. 2012.
[25] J. He, Y. W. Li, J. M. Guerrero, J. C. Vasquez, and F. Blaabjerg, "An islanded microgrid reactive power sharing scheme enhanced by programmed virtual impedances," in *Proc. IEEE Int. Symp. Power Electron. Distrib. Gener. Syst.*, 2012, pp. 229–235.
[26] J. He, Y. W. Li, J. M. Guerrero, F. Blaabjerg, and J. C. Vasquez, "An islanding microgrid power sharing approach using enhanced virtual impedance control scheme," *IEEE Trans. Power Electron.*, vol. 28, no. 11, pp. 5272–5282, Nov. 2013.
[27] Y. Zhang and H. Ma, "Theoretical and experimental investigation of networked control for parallel operation of inverters," *IEEE Trans. Ind. Electron.*, vol. 59, no. 4, pp. 1961–1970, Apr. 2012.
[28] C.-T. Lee, C.-C. Chu, and P.-T. Cheng, "A new droop control method for the autonomous operation of distributed energy resources interface converters," *IEEE Trans. Power Electron.*, vol. 28, no. 4, pp. 1980–1993, Apr. 2013.
[29] A. M. Roslan, K. H. Ahmed, S. J. Finney, and B. W. Williams, "Improved instantaneous average current-sharing control scheme for parallel-connected inverter considering line impedance impact in microgrid networks," *IEEE Trans. Power Electron.*, vol. 26, no. 3, pp. 702–716, Mar. 2011.
[30] Q. Shafiee, J. M. Guerrero, and J. C. Vasquez, "Distributed secondary control for islanded microgrids—A novel approach," *IEEE Trans. Power Electron.*, vol. 29, no. 2, pp. 1018–1031, Feb. 2014.
[31] E. A. A. Coelho, P. C. Cortizo, and P. F. D. Garcia, "Small-signal stability for parallel-connected inverters in stand-alone AC supply systems," *IEEE Trans. Ind. Appl.*, vol. 38, no. 2, pp. 533–542, Mar./Apr. 2002.
[32] H. J. Avelar, W. A. Parreira, J. B. Vieira, L. de Freitas, and E. A. A. Coelho, "A state equation model of a single-phase grid-connected inverter using a droop control scheme with extra phase shift control action," *IEEE Trans. Ind. Electron.*, vol. 59, no. 3, pp. 1527–1537, Mar. 2012.
[33] E. A. A. Coelho, P. C. Cortizo, and P. F. D. Garcia, "Small signal stability for single phase inverter connected to a stiff AC system," in *Proc. IEEE 34th Ind. Appl. Conf.*, 1999, pp. 2180–2187.

Hisham Mahmood (S'10) received the M.E.Sc. degree in control engineering from Lakehead University, ON, Canada, in 2008. He is currently working toward the Ph.D. degree with the Department of Electrical and Computer Engineering, Western University, London, ON, Canada.

His research interests include modeling and control of switching power converters, distributed generation, renewable energy interface, microgrids, and power quality.

Dennis Michaelson (M'12) received the B.A.Sc. degree in automation engineering from Simon Fraser University, BC, Canada, in 1993. He is currently working toward the Ph.D. degree in the Department of Electrical and Computer Engineering, Western University, London, ON, Canada.

He was the Vice-President of Engineering for EK3 Technologies, Inc., where he led a team developing networked embedded systems for commercial multimedia applications. His research interests include the control of energy storage in microgrids, power electronic converters, mobile robotics, and embedded real-time systems.

Jin Jiang (S'85–M'87–SM'94) received the Ph.D. degree from the University of New Brunswick, Saint John, NB, Canada, in 1989.

Since 1991, he has been with the Department of Electrical and Computer Engineering, University of Western Ontario, London, Canada, where he is currently a Senior Industrial Research Chair Professor. His research interests include fault-tolerant control of safety-critical systems, advanced control of electrical power plants, and power systems involving renewable energy resources.

Dr. Jiang is a Fellow of Canadian Academy of Engineering. He is also a Member of the International Electrotechnical Commission (IEC) 45A subcommittee to develop industrial standards on instrumentation and control for nuclear facilities. He also works closely with the International Atomic Energy Agency (IAEA) on modern control and instrumentation for nuclear power plants.